Self-Assembly of Helical Nanofibrous Chiral Covalent Organic Frameworks

Xihao Tang, Xiangji Liao, Xinting Cai, Jialin Wu, Xueying Wu, Qianni Zhang, Yilun Yan, Shengrun Zheng, Huawei Jiang, Jun Fan, Songliang Cai,* Weiguang Zhang* and Yi Liu*

Abstract: Despite significant progress on the design and synthesis of covalent organic frameworks (COFs), precise control over microstructures of such materials remains challenging. Herein, two chiral COFs with well-defined one-handed double-helical nanofibrous morphologies were constructed via an unprecedented template-free method, capitalizing on the diastereoselective formation of aminal linkages. Detailed time-dependent experiments reveal the spontaneous transformation of initial rod-like aggregates into the double-helical microstructures. We further demonstrated that the helical chirality and circular dichroism signal can be facilely inversed by simply adjusting the amount of acetic acid during synthesis. Moreover, by transferring chirality to achiral fluorescent molecular adsorbents, the helical COF nanostructures can effectively induce circularly polarized luminescence with the highest luminescent asymmetric factor (g_{lum}) up to ~ 0.01.

Introduction

Helicity is not only one of the most important structural properties of biological macromolecules, but also a universal feature that exists in nature across the molecular scale to macroscopic scale. Inspired by nature, great efforts have been devoted to constructing helical materials at different scales, such as microscopically visible oligomers[1] and polymers[2] with helical molecular conformations, mesoscopic helical nanostructures based on metals,[3] inorganic molecules[4] and supramolecular gels,[5] and macroscopically discernible biomimetic helical materials.[6] The highly ordered helical topologies endow these materials with unique physical and chemical properties.[7]

[*] Dr. X. Tang, X. Cai, J. Wu, Q. Zhang, Y. Yan, Prof. S. Zheng, Prof. H. Jiang, Prof. J. Fan, Prof. S. Cai, Prof. W. Zhang
GDMPA Key Laboratory for Process Control and Quality Evaluation of Chiral Pharmaceuticals, and Guangzhou Key Laboratory of Analytical Chemistry for Biomedicine
School of Chemistry, South China Normal University
Guangzhou, 510006 (China)
E-mail: songliangcai@m.scnu.edu.cn
wgzhang@scnu.edu.cn
Dr. Y. Liu
The Molecular Foundry
Lawrence Berkeley National Laboratory
Berkeley, California, 94720 (United States)
E-mail: yliu@lbl.gov
X. Liao
State Key Laboratory of Coordination Chemistry
School of Chemistry and Chemical Engineering, Nanjing University
Nanjing, 210023 (China)
Prof. S. Zheng, Prof. H. Jiang, Prof. J. Fan, Prof. S. Cai, Prof. W. Zhang
SCNU Qingyuan Institute of Science and Technology Innovation Co., Ltd.
Qingyuan, 511517 (China)

As a new member of crystalline porous materials, covalent organic frameworks (COFs) have shown broad applications such as gas adsorption,[8] chemical sensing,[9] asymmetric catalysis,[10] and chromatographic separation,[11] owing to their outstanding features such as tunable pore structures, high surface areas and excellent chemical stability. To explore the structure-property relationship for practical applications, COFs with various fundamental morphologies such as nanofibers,[12] nanotubes,[13] nanospheres,[14] core-shell,[15] and nanosheets[16] have been explored. However, COFs with single-handedness double helices remain unexplored despite their potential applications in the fields of chiral recognition, chiral catalysis, and chiral optical devices.[7a] On the other hand, several attempts towards helical framework materials have been reported involving the related metal organic frameworks (MOFs). For instance, MOFs with helical superstructures were obtained using a template-assisted approach.[17] However, the initial introduction and final removal of the templates demanded additional efforts to retain the helical MOF crystalline phase without disruption. Recently, the fabrication of layered helical tubular MOFs by a self-template method has also been reported.[18] Due to the lack of chiral induction, racemization occurred with both left-handed and right-handed twisted tubes in the crystalline product. As such, development of a facile and template-free strategy for the assembly of COFs with helical morphologies and chiroptical properties is highly desirable.

Herein, we report the design and synthesis of an enantiomeric pair of chiral helical COFs, namely ***L*-PDC-TZ COF** and ***D*-PDC-TZ COF,** by utilizing (*S*)- and (*R*)-3-amino-4-oxo-2-(pyrrolidin-2-yl)-3,4-dihydroquinazoline-7-carbohydrazide (***L*-PDC** and ***D*-PDC**) and 4,4',4''-(1,3,5-triazine-2,4,6-triyl)tribenzaldehyde (**TZ**) as the building blocks (Scheme 1). The chiral framework formation involves both an unprecedented aminal linkage and a hydrazone linkage, formed between the polyfunctional ***L/D*-PDC** with benzaldehyde (**BA**), as supported by the formation of diastereomeric ***L/D*-PDC-BA** from the corresponding model reactions (Scheme 1). Under same synthetic conditions, the two chiral COFs displayed opposite Cotton effects and unique left-handed and right-handed double-helical morphologies, indicating the enantiomeric nature of each other. Detailed mechanistic studies reveal the time-dependent self-assembly process of the COF-based double-helical nanofibers. Interestingly, by adjusting the amount of acetic acid employed in the synthesis, the COF nanostructures can be switched between the two opposite helicities, thereby enabling the control over framework chirality and helicity. This work presents an unprecedented example of template-free self-assembly of chiral nanofibrous COF double-helices. We have further demonstrated modulated chiroptical properties of the nanofibrous chiral COF helices. When achiral chromophores are impregnated into the framework, induced

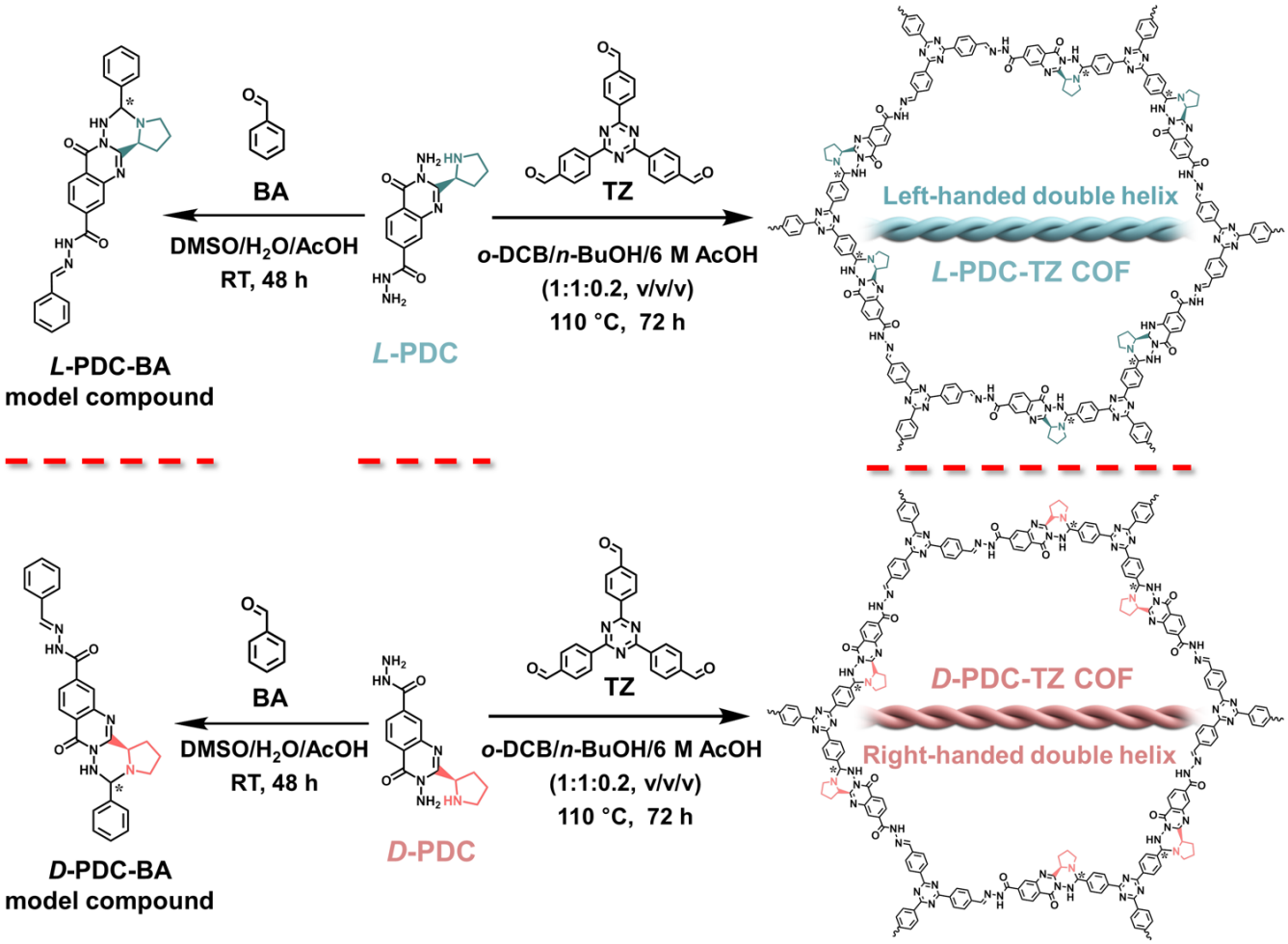

Scheme 1. Syntheses of the model compounds ***L*-PDC-BA** and ***D*-PDC-BA** at room temperature, as well as ***L*-PDC-TZ COF** and ***D*-PDC-TZ COF** from reactions in *o*-DCB/*n*-BuOH/6 M AcOH (1:1:0.2, v/v/v) at 110 °C for 72 h. The asterisks (*) indicate the newly formed chiral centers.

circularly polarized luminescence (CPL) activities of the external chromophore have been achieved.

Results and Discussion

The chiral monomers ***L*-PDC** and ***D*-PDC** were synthesized by the amidation of dimethyl 2-aminoterephthalate with proline and a further acylation step (Scheme S1). Due to an unexpected ring-closure process,[19] dissymmetric hydrazide linkers bearing a quinazoline unit and a chiral pyrrolidinyl side chain were obtained. Single crystal X-ray diffraction (SC-XRD) analysis confirmed the absolute configuration of ***L*-PDC** as reflected by a reasonable Flack parameter (Figure S1 and Table S1),[20] while CD spectra demonstrated the enantiomeric nature of ***L*-PDC** and ***D*-PDC** (Figure S2a). The corresponding racemate compound (***Rac*-PDC**) was prepared by recrystallization of equal amounts of ***L*-PDC** and ***D*-PDC** in methanol. The model compounds ***L*-PDC-BA** or ***D*-PDC-BA** were synthesized from the condensation reaction between ***L*-PDC** or ***D*-PDC** and **BA**, respectively (Schemes 1 and S2). The two hydrazide groups within ***L*/*D*-PDC** displayed different reactivities towards **BA**, with one transforming to a conventional hydrazone, and the other undergoing diastereoselective cyclocondensation together with the appended pyrrolidine group to give a saturated triazine ring structure that is annulated to the dihydroquinazoline core. Similar to those of the ***L*-PDC** and ***D*-PDC** monomers, the CD spectra of the model compounds ***L*-PDC-BA** and ***D*-PDC-BA** displayed mirror images of each other (Figure S2b), implying that they were also a pair of enantiomers. The ring-closing reaction mechanism of the model compound ***L*-PDC-BA** was proposed (Scheme S3). The reaction of ***L*-PDC** with **BA** could firstly produce the dihydrazone intermediate. In the presence of acetic acid, the imine bonds of the dihydrazone intermediate can be activated through protonation of the nitrogen atoms. The nucleophilic attack of the lone pair electrons on the nitrogen atom of pyrrolidine towards the nearby C=N bond furnishes a triazine ring and a newly generated chiral center, leading to the formation of the ring-closed ***L*-PDC-BA** product containing aminal linkage. The diastereoselectivity between the two isomers, as well as the absolute configuration of the major isomer of ***L*-PDC-BA** from the reaction between ***L*-PDC** and **BA**, was verified by proton and carbon nuclear magnetic resonance (^{1}H NMR and ^{13}C NMR) spectroscopies and SC-XRD analysis (Figure S3 and Table S1).[20] By adjusting the AcOH loading during syntheses, the ratio of the two

diastereomers could be altered significantly from 1:6.4 to 1:0.9 (Figure S4, also see discussions in later section). In addition, when the two diastereomers of ***L*-PDC-BA** in different ratios were treated with trifluoroacetic acid, identical ring-opened dihydrazone products were obtained, confirming the dynamic nature of the diastereomeric triazine unit in ***L*-PDC-BA** (Scheme S4 and Figure S5). Following a similar ring-closing protocol, the reaction between ***L*-/*D*-PDC** and **TZ** could give rise to ***L*-/*D*-PDC-TZ COF** with novel chiral aminal linkages (Scheme 1). In a typical procedure for COF synthesis, ***L*-PDC-TZ COF** was synthesized by condensing ***L*-PDC** with **TZ** in *o*-DCB/*n*-BuOH/6 M AcOH (1:1:0.2, v/v/v) at 110 °C for 72 h (Scheme 1). ***D*-PDC-TZ COF** and ***Rac*-PDC-TZ COF** were prepared by following the exact same procedure except that the ***D*-PDC** and ***Rac*-PDC** were used, respectively. It is worth noting that development of COFs with new linkages can engender fascinating structures and interesting properties,[16, 21] however the synthesis scope still remains significantly limited, especially for those constructed based on cascade reactions.[22]

To investigate the crystallinity of the obtained COFs, powder X-ray diffraction (PXRD) studies and theoretical simulations were conducted. The experimental PXRD profile showed that the three COFs were crystalline and exhibited the same diffraction peaks appeared at around 2.36°, 4.78° and 26.0° (Figure 1a), corresponding to the 100, 110 and 001 plane reflections, respectively. Representatively, the simulated diffraction pattern indicated that the AA stacking mode (Figure 1b) provided a better description of ***L*-PDC-TZ COF** than that of the AB stacking mode (Figure S6). The unit cell parameters given by the Pawley refinement were $a = b = 43.12$ Å, $c = 4.117$ Å, $\alpha = \beta = 90°$, and $\gamma = 120°$, with $R_p = 8.47\%$, and $R_{wp} = 6.40\%$. The Fourier transform infrared (FT-IR) spectra showed the nearly complete disappearance of the aldehyde (1703 cm^{-1}) and amino vibrations

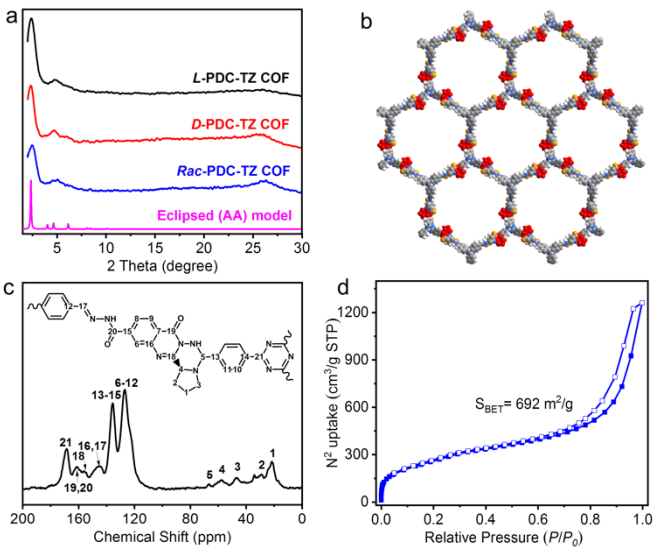

Figure 1. (a) Experimental PXRD patterns of ***L*-PDC-TZ COF** (black), ***D*-PDC-TZ COF** (red), ***Rac*-PDC-TZ COF** (blue) and simulated pattern (pink). (b) Simulated structure of ***L*-PDC-TZ COF** with AA stacking. (c) ^{13}C CP/MAS NMR spectrum of ***L*-PDC-TZ COF**. (d) Nitrogen adsorption (filled symbols) and desorption (empty symbols) isotherms of ***L*-PDC-TZ COF**.

(3200- 3400 cm^{-1}) along with the emergence of C=N characteristic of ***L*-PDC** with **TZ** to form ***L*-PDC-TZ COF** (Figure S7). Similar spectral feature changes were observed for the model compound ***L*-PDC-BA**. More chemical information was obtained from the solid-state ^{13}C cross-polarization magic-angle spinning (CP/MAS) NMR analysis (Figure 1c). The resonances at 21, 29, 47, and 57 ppm were assigned to the pyrrolidine moieties, and the resonance at 66 ppm was attributed to the aminal carbon. Moreover, the resonances at 156 and 161 ppm confirmed the presence of the quinazolinone units. The detailed assignment of ^{13}C NMR chemical shifts for ***L*-PDC-TZ COF** was depicted in Figure 1c. The porosity and surface area of ***L*-PDC-TZ COF** were evaluated by measuring the nitrogen adsorption-desorption isotherms at 77 K. Prior to the porosity test, ***L*-PDC-TZ COF** was treated by exchanging the guest solvents with MeOH, and activated by supercritical CO_2 (see Supporting Information). The Brunauer−Emmett−Teller (BET) surface area of the resulting COF was determined to be 692 m^2/g (Figure 1d), which is on par with some of the recently reported COFs bearing novel linkages[16, 21] The presence of hysteresis loops and the pore size distribution estimated by the quenched solid density functional theory (QSDFT) model showcased the abundant mesopores of ~2.8 nm within ***L*-PDC-TZ COF**, which was in good agreement with the predicted value (2.9 nm, Figure S8). Thermal gravimetric analysis (TGA) under a nitrogen atmosphere revealed that ***L*-PDC-TZ COF** was thermally stable up to 330 °C (Figure S9).

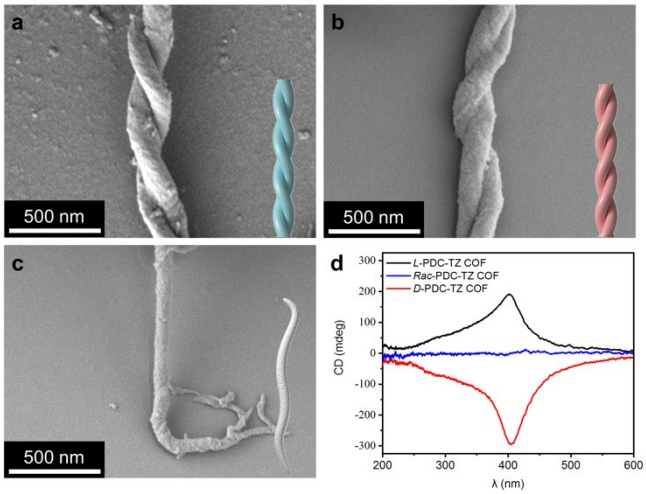

Figure 2. SEM images of (a) ***L*-PDC-TZ COF**, (b) ***D*-PDC-TZ COF** and (c) ***Rac*-PDC-TZ COF** synthesized in *o*-DCB/*n*-BuOH/6 M AcOH (1:1:0.2, v/v/v) at 110 °C for 72 h. Insets are cartoon representations of the fibrous structures. (d) CD spectra of ***L*-PDC-TZ COF** (black), ***D*-PDC-TZ COF** (red) and ***Rac*-PDC-TZ COF** (blue).

Morphological studies by subsequent scanning electron microscopy (SEM) revealed that the as-synthesized chiral COFs predominantly assembled into well-defined double-helical nanofibrous structures. Synthesized by the typical procedure, ***L*-PDC-TZ COF** displayed left-handed double helicity (Figures 2a and S10a), whereas ***D*-PDC-TZ COF** showed right-handed double helicity (Figures 2b and S10b). The pitches and the diameters of both helices were around 500 and 270 nm, respectively, whereas the diameter of each individual strand was about 110 nm. In contrast, ***Rac*-PDC-TZ COF** was obtained as single fibers with a

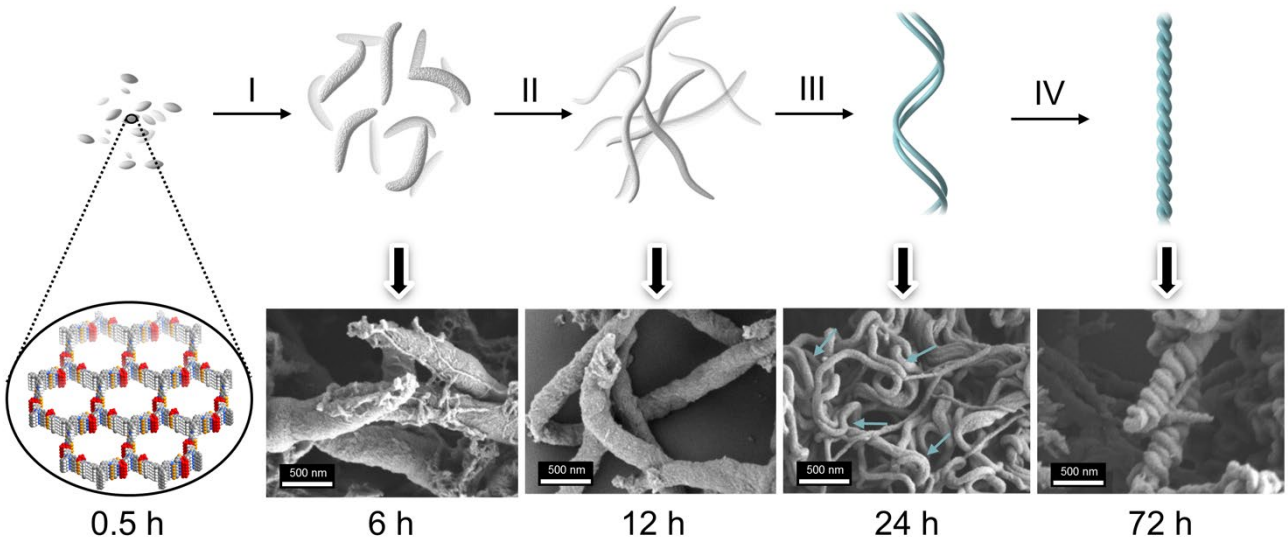

Figure 3. Proposed mechanism for double helices formation of ***L*-PDC-TZ COF**: (i) Formation of rod-like aggregates. (ii) Transformation of rods into fibers. (iii) Directional entanglement and twist of two adjacent fibers. The blue arrows indicate the preliminary signs of entanglement. (iv) Materialization of the double helices.

diameter of 60 nm, showing no helicity (Figures 2c and S10c). Transmission electron microscopy (TEM) images clearly demonstrated the non-hollow nature and the helicity of the obtained helices (Figure S11). To shed light on batch-to-batch reproducibility and consistency, low-magnification SEM images of three different batches of ***L*-PDC-TZ COF** were acquired (Figure S12). It is apparent that double helices were persistently the major product, and the formation of such structures was repeatable and not contingent. In addition, SEM images of three different batches of ***D*-PDC-TZ COF** (Figure S13) revealed the formation of double helices with right-handed helicity, opposite to that of ***L*-PDC-TZ COF**. The dominant presence of left- and right-handed helical structures from the respective ***L*-** and ***D*-PDC-TZ COFs** provides strong support for the general and chiral selective formation of double helices. Solid-state circular dichroism (CD) spectral measurements were performed to evaluate the chirality of the three COFs. ***L*-PDC-TZ COF** exhibits a positive Cotton effect at 401 nm (Figure 2d, black line), suggesting that the chirality of the localized chiral center is transferred to the framework. The CD spectrum of ***D*-PDC-TZ COF** shows a mirror image to that of ***L*-PDC-TZ COF**, indicating the enantiomeric nature of each other. As expected, ***Rac*-PDC-TZ COF** displays no Cotton effect. Although COFs with diverse morphologies have been reported,[12-16, 23] to the best of our knowledge, ***L*-PDC-TZ COF** and ***D*-PDC-TZ COF** present the first examples of chiral COFs with a helical nanofibrous morphology.

To shed light onto the formation mechanism of the double helices, time-dependent morphological studies were performed by quenching COF reaction mixtures at different time intervals. Taking ***L*-PDC-TZ COF** as an example, SEM images of the product taken after 0.5 h indicated the formation of small fusiform crystallites (Figure S14a). The minor diffraction peaks at ~4.8° in PXRD pattern proved the crystalline nature of the crystallites (Figure S15). The peak appeared at around 400 nm in the CD spectrum was designated as the characteristic peak of ***L*-PDC-TZ COF** (Figure S16). After 6 h (process I in Figure 3), short rods with rough and irregular surfaces were observed (Figure S14b). When the reaction time was prolonged to 12 to 24 h (processes II and III in Figure 3), uniform elongated fibers were observed along with some preliminary signs of entanglement (Figures S14c and S14d). In 72 h (process IV in Figure 3), double helices were isolated as the major product with some remaining unentangled fibers (Figure S14e). Further increase of the reaction time up to 168 h led to no obvious changes in SEM (Figure S13f) images, PXRD (Figure S15) and CD (Figure S16) spectra, indicating the thermodynamic stability of the helices. Based on above results, the following self-assembly mechanism for the double-helice formation was proposed (Figure 3). Initially, the fast-forming crystallites agglomerate into rod-like aggregates, as evident by the rough surfaces and irregular shapes. Subsequently, the condensation of reactive amines and aldehydes at the interfaces with unreacted precursors leads to grain boundary fusion, resulting in anisotropic morphological changes such as the desirable diameter reduction and length increase.[13] The observed enhanced crystallinity supports this transformation (Figure S15). When the flexible and regular fibers are long enough, two adjacent fibers begin to twist and entangle to form the helical structures with preferential handedness that is presumably dictated by the periodically distributed chiral moieties.[24] Recent study has related similar entanglement to solvophobic effects and inter-fiber interactions.[25] This assumption is also supported by the similarity of diameters for the uniform fibers and the strands of the helices. Well-defined double helices are materialized at the final growth stage. It is worth mentioning that due to the extended length and flexibility of the fibers, the self-assembled helices inevitably became entangled with each other and could not be dispersed well (Figure S12). The fibers with high aspect ratio and flexibility were more favorable in the self-assembly of COF helices than the originating short and thick rods, which was consistent with the recently reported helical MOF superstructures.[18] In the case of ***Rac*-PDC-TZ COF**, fiber growth is free of chiral twist due to the mesomeric effect of the framework, thus no helical fibers and double helices are formed.

Intriguingly, we found that both the chirality and the helicity of the chiral COFs could be inversed by adjusting the amount of

AcOH used during the synthesis. When the volume ratio of AcOH in the solvent mixture of *o*-DCB/*n*-BuOH/6 M AcOH was decreased from 1:1:0.2 to 1:1:0.1, the CD spectrum of ***L*-PDC-TZ COF** exhibited a negative Cotton effect (Figure 4a), while the SEM images showed a right-handed helical fibrous morphology (Figure S17). Both chirality and helicity were the mirror counterparts of ***L*-PDC-TZ COF** prepared using higher loading of AcOH, indicating the occurrence of helix inversion. Such an inversion was likewise confirmed in the case of ***D*-PDC-TZ COF**, which also indicates that while the chirality of the linker doesn't dictate the helicity, the CD chirality and the helical morphology of the frameworks are persistently correlated, that is, negative Cotton effect correlates with right handedness and positive Cotton effect correlates with left handedness. To further elucidate the phenomenon, time-dependent experiments were conducted. With further extension of reaction time up to 168 h, the CD spectra and morphologies of ***L*-PDC-TZ COF** prepared using 1:1:0.05 *o*-DCB/*n*-BuOH/AcOH were nearly identical to those obtained in 72 h (Figures S17 and S18). These results supported the thermodynamic stability of both left-handed and right-handed ***L*-PDC-TZ COF**. No evidence of interconversion between the two, as was often reported in supramolecular assemblies.[26] Moreover, diffraction peak positions in PXRD patterns showed negligible difference for those synthesized at different loading of AcOH (Figure S19), suggesting that there is no difference in framework periodicity or inter-layer stacking mode.[27] We postulate that the AcOH-dependent chirality inversion is due to the acid-biased diastereoselectivity expressed in the highly dynamic triazine ring systems. Such acid susceptibility was verified by following the diastereoselectivity changes during the formation of ***L*-PDC-BA** at different AcOH loadings using ^{1}H NMR spectroscopy (Scheme S2 and Figure S4). When the volume ratio of AcOH in DMSO/H_2O solution was increased from 0% to 33%, the ratio of the resultant two diastereomers, determined by ^{1}H NMR spectroscopy, changed significantly from 1:6.4 to 1:0.9 (Figure S4), indicating inverted chirality of the aminal carbon under the influence of AcOH. Such acid-dependent chiral selectivity changes may have occurred and amplified throughout the COF frameworks, and is consistent with the observed helix inversion, as illustrated in Figure 4c.

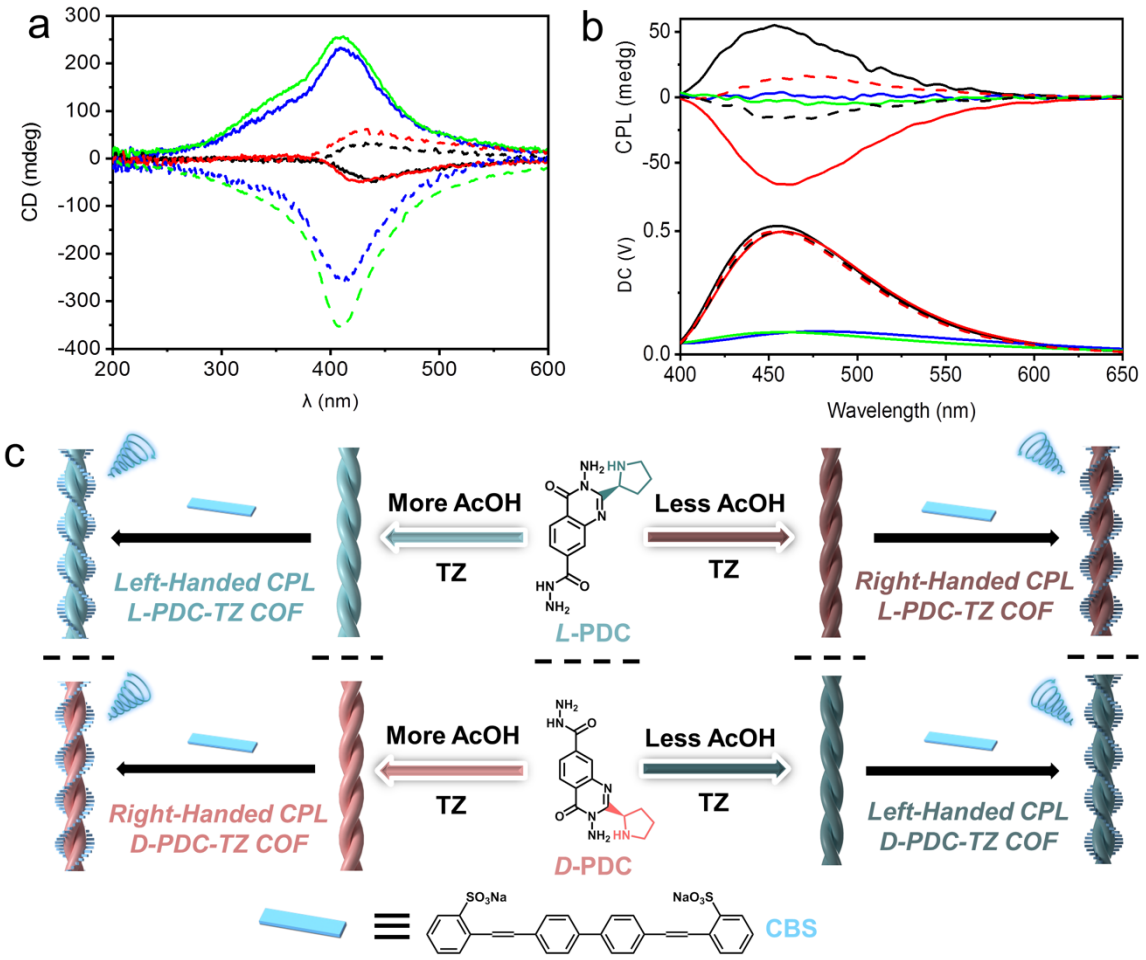

Figure 4. (a) CD spectra of ***L*-PDC-TZ COF** (solid line) and ***D*-PDC-TZ COF** (dashed line) prepared at different volume ratios of AcOH in the solvent mixture of *o*-DCB/*n*-BuOH/6 M AcOH for 72 h: 1:1:0.05 (black), 1:1:0.1 (red), 1:1:0.2 (blue), 1:1:0.3 (green). (b) CPL spectra of ***L*-PDC-TZ COF@CBS** (black), ***D*-PDC-TZ COF@CBS** (red), ***L*-PDC-TZ COF** (blue) and ***D*-PDC-TZ COF** (green) dispersed in water, where COFs were prepared using *o*-DCB/*n*-BuOH/6 M AcOH (1:1:0.2), together with CPL spectra of ***L*-PDC-TZ COF@CBS** (black dash), ***D*-PDC-TZ COF@CBS** (red dash) dispersed in water, where COFs were prepared using *o*-DCB/*n*-BuOH/6 M AcOH (1:1:0.1). The DC value in the bottom spectrum represents the corresponding fluorescence intensity. (c) Schematics summarizing the tunable chirality, helicity, and CPL activity of ***L*-** and ***D*-PDC-TZ COF@CBS** materials.

The intrinsic chirality and unique mesoscopic helical morphology of those COFs inspired their use for engineering chiroptical properties, especially the circularly polarized luminescence (CPL). While numerous chiral materials have been exploited for CPL properties, COF-based materials are just on the horizon, with both of the known examples based on chiral COF nanosheets wherein mechanical exfoliation may result in a decrease in crystallinity and porosity.[28] Herein, we presented a different strategy, that is, using helical nanofibrous COFs as the chiral source to induce CPL activity of achiral, physiosorbed fluorescent molecules, thus obviating the need of exfoliation and covalent attachment of chromophores (Figure 4c). As shown in Figure 4b and Figure S20, both the left-handed helical ***L*-PDC-TZ COF** and right-handed helical ***D*-PDC-TZ COF** were weakly fluorescent and almost CPL silent, owing to fluorescence quenching caused by strong π–π stacking between the neighboring COF layers. Anticipating that the presence of abundant pore channels would allow the intake of chromophores by noncovalent interactions and lead to induced CPL, disodium 4,4'-bis(2-sulfonatostyry)biphenyl (**CBS**), a typical fluorescent dye, was therefore used for loading into the chiral helical COFs. Photoluminescent studies indicated that the addition of **CBS** to the ***L*-** and ***D*-PDC-TZ COF** suspensions gave rise to enhanced fluorescent intensities, indicating the strong interactions between helical COFs and **CBS** molecules (Figure S20). The **CBS** loaded helical COF materials, namely ***L*-** and ***D*-PDC-TZ COF@CBS**, were then prepared by immersing ***L*-** and ***D*-PDC-TZ COF** into the **CBS** aqueous solution for 12 h at room temperature. The obtained chiral helical **COF@CBS** materials exhibited intense CPL signals (Figure 4b). The left-handed helical ***L*-PDC-TZ COF@CBS** displayed a positive CPL peak at 450 nm, while the right-handed helical ***D*-PDC-TZ COF@CBS** showed a negative CPL peak at the same wavelength (Figure 4b). Besides, the peaks at 450 nm in nonpolarized fluorescence spectra of ***L*-** and ***D*-PDC-TZ COF@CBS** were consistent with the CPL emission peaks. The corresponding $|g_{lum}|$ luminescent asymmetric factors were found to be 6.8×10^{-3} and 9.5×10^{-3}, respectively (Figure S21). The variation in the CPL intensities and $|g_{lum}|$ factors of ***L*-** and ***D*-PDC-TZ COF@CBS** may be caused by the CD signal differences of the two COFs (Figure 2d). These results indicated that the chiral COF double helices could transfer and amplify their helicity to the achiral fluorescent molecules, consequently emitting strong CPL signals. Moreover, when the helicity was inverted by adjusting the amount of AcOH used in the reaction, the CPL signals could also be inverted, which was consistent with the CD and imaging results, albeit with reduced CPL intensity (Figure 4b) due to the decreased crystallinity (Figure S19) and CD intensities (Figure 4a). The corresponding $|g_{lum}|$ factors of the right-handed helical ***L*-PDC-TZ COF@CBS** and the left-handed helical ***D*-PDC-TZ COF@CBS** were found to be 1.5×10^{-3} and 2.5×10^{-3}, respectively (Figure S21).

Conclusion

We have demonstrated an unprecedented example of double-helical nanofibrous chiral COFs, produced by a single-step, template-free method involving a chiral cyclic aminal linkage. Time-dependent studies supported the transformation of initial rod-like COF aggregates into elongated fibers, followed by directional self-assembly into double helices with single handedness. Through simply tuning monomer chirality or the amount of acetic acid during synthesis, the chirality and helicity of the resulting COF double helices can be altered. Detailed studies on model reactions have revealed the formation of chiral triazine ring systems from cyclocondensation and the associated acid-biased diastereoselectivity changes, correlating with the observed chirality inversion in the COF helices. Those helical COF nanostructures can transfer their mesoscopic helical sense to achiral fluorescent molecules through physisorption, resulting in amplified circularly polarized luminescence. This work not only provides new linking chemistry and fresh insights into the self-assembly mechanism of chiral helical COFs, but also opens a scalable strategy for the development of novel COF-based CPL materials.

Acknowledgements

We gratefully acknowledge the financial support from the National Natural Science Foundation of P. R. China (Grant Nos. 22171092, 92056113 and 22073032), the Natural Science Foundation of Guangdong Province (Grant Nos. 2021A1515010211 and 2022A1515011243), and the Science and Technology Program of Guangzhou (Grant No. 202102020667), as well as the Shenzhen Science and Technology Program (Grant No. CJGJZD20210408091800002). We also thank Prof. Youxuan Zheng at Nanjing University for help with CPL measurements. Y.L. acknowledges the support from the Molecular Foundry, a user facility supported by the Office of Science, Office of Basic Energy Sciences, of the U.S. Department of Energy under Contract No. DE-AC02-05CH11231.

Conflict of Interest

The authors declare no conflict of interest.

Data Availability Statement

The data that support the findings of this study are available in the Supporting Information of this article.

Keywords: chiral covalent organic frameworks • chiral inversion • circularly polarized luminescence • helical nanofibrous morphology

[1] C. Lang, X. Deng, F. Yang, B. Yang, W. Wang, S. Qi, X. Zhang, C. Zhang, Z. Dong, J. Liu, *Angew. Chem. Int. Ed.* **2017**, *56*, 12668.

[2] a) D. Hirose, A. Isobe, E. Quiñoá, F. Freire, K. Maeda, *J. Am. Chem. Soc.* **2019,** *141*, 8592-8598.; b) W. Makiguchi, S. Kobayashi, Y. Furusho, E. Yashima, *Angew. Chem. Int. Ed.* **2013**, *52*, 5275-5279.

[3] M. Nakagawa, T. Kawai, *J. Am. Chem. Soc.* **2018**, *140*, 4991-4994.

[4] S. Che, Z. Liu, T. Ohsuna, K. Sakamoto, O. Terasaki, T. Tatsumi, *Nature* **2004**, *429*, 281-284.

[5] H. Jiang, Y. Jiang, J. Han, L. Zhang, M. Liu, *Angew. Chem., Int. Ed.* **2019**, *58*, 785-790.

[6] G. M. Spinks, *Adv. Mater.* **2020**, *32*, 1904093.

[7] a) X. Han, C. Yuan, B. Hou, L.-J. Liu, H.-Y. Li, Y. Liu, Y. Cui, *Chem. Soc. Rev.* **2020**, *49*, 6248-6272; b) T. Leigh, P. Fernandez-Trillo, *Nat. Rev. Chem.* **2020,** *4*, 291-310; c) Y. Zhang, S. Yu, B. Han, Y. Zhou, X. Zhang, X. Gao, Z. Tang, *Matter* **2022**, *5*, 837-875.

[8] a) C. J.Doonan, D. J. Tranchemontagne, T. G. Glover, J. R. Hunt, O. M. Yaghi, *Nat. Chem.* **2010**, *2*, 235-238; b) S.-L. Cai, K. Zhang, J.-B. Tan, S. Wang, S.-R. Zheng, J. Fan, Y. Yu, W.-G. Zhang, Y. Liu, *ACS Macro Lett.* **2016**, *5*, 1348-1352.

[9] a) S.-Y. Ding, M. Dong, Y.-W. Wang, Y.-T. Chen, H.-Z. Wang, C.-Y. Su, W. Wang, *J. Am. Chem. Soc.* **2016**, *138*, 3031-3037; b) G. Chen, H.-H.

Lan, S.-L. Cai, B. Sun, X.-L. Li, Z.-H. He, S.-R. Zheng, J. Fan, Y. Liu, W.-G. Zhang, *ACS Appl. Mater. Interfaces* **2019**, *11*, 12830-12837.

[10] a) H. Xu, J. Gao, D. Jiang, *Nat. Chem.* **2015**, *7*, 905-912; b) H.-S. Xu, S.-Y. Ding, W.-K. An, H. Wu, W. Wang, *J. Am. Chem. Soc.* **2016**, *138*, 11489-11492; c) H.-C. Ma, J.-L. Kan, G.-J. Chen, C.-X. Chen, Y.-B. Dong, *Chem. Matter.* **2017**, *29*, 6518-6524; d) X. Han, J. Zhang, J. Huang, X. Wu, D. Yuan, Y. Liu, Y. Cui, *Nat. Commun.* **2018**, *9*, 1294.

[11] a) H.-L. Qian, C.-X. Yang, X.-P. Yan, *Nat. Commun.* **2016**, *7*, 12104; b) K. Zhang, S.-L. Cai, Y.-L. Yan, Z.-H. He, H.-M. Lin, X.-L. Huang, S.-R. Zheng, J. Fan, W.-G. Zhang, *J. Chromatogr. A* **2017**, *1519*, 100-109; c) X. Han, J. Huang, C. Yuan, Y. Liu, Y. Cui, *J. Am. Chem. Soc.* **2018**, *140*, 892-895.

[12] K. Dey, S. Bhunia, H. S. Sasmal, C. M. Reddy, R. Banerjee, *J. Am. Chem. Soc.* **2021**, *143*, 955-963.

[13] B. Gole, V. Stepanenko, S. Rager, M. Grüne, D. D. Medina, T. Bein, F. Würthner, F. Beuerle, F., *Angew. Chem., Int. Ed.* **2018**, *57*, 846-850.

[14] W. Ma, Q. Zheng, Y. He, G. Li, W. Guo, Z. Lin, L. Zhang, *J. Am. Chem. Soc.* **2019**, *141*, 18271-18277.

[15] G. Zhang, M. Tsujimoto, D. Packwood, N. T. Duong, Y. Nishiyama, K. Kadota, S. Kitagawa, S. Horike, *J. Am. Chem. Soc.* **2018,** *140*, 2602-2609.

[16] S. Mitra, S. Kandambeth, B. P. Biswal, A. Khayum M, C. K. Choudhury, M. Mehta, G. Kaur, S. Banerjee, A. Prabhune, S. Verma, S. Roy, U. K. Kharul, R. Banerjee, *J. Am. Chem. Soc.* **2016**, *138*, 2823-2828.

[17] H. Wang, W. Zhu, J. Li, T. Tian, Y. Lan, N. Gao, C. Wang, M. Zhang, C. F. J. Faul, G. Li, *Chem. Sci.* **2015**, *6*, 1910-1916.

[18] L. Feng, J.-L. Li, G. S. Day, X.-L. Lv, H.-C. Zhou, *Chem* **2019**, *5*, 1265-1274.

[19] M. T. H. Khan, R. Khan, Y. Wuxiuer, M. Arfan, M. Ahmed, I. Sylte, *Bioorg. Med. Chem.* **2010**, *18*, 4317-4327.

[20] CCDC Deposition Numbers 2165889 (for ***L*-PDC**) and 2184581 (for ***L*-PDC-BA**) contain the supplementary crystallographic data for this paper. These data can be acquired free-of-charge *via* www.ccdc.cam.ac.uk/data_request/cif, or by emailing data-request@ccdc.cam.ac.uk, or by contacting the Cambridge Crystallographic Data Centre, 12 Union Road, Cambridge CB2 1EZ, UK; fax: +44 1223 336033.

[21] a) X. Li, H. Wang, H. Chen, Q. Zheng, Q. Zhang, H. Mao, Y. Liu, S. Cai, B. Sun, C. Dun, M. P. Gordon, H. Zheng, J. A. Reimer, J. J. Urban, J. Ciston, T. Tan, E. M. Chan, J. Zhang, Y. Liu, *Chem* **2020**, *6*, 933-944; b) Y. Jiang, H. Jung, S. H. Joo, Q. K. Sun, C. Li, H.-J. Noh, I. Oh, Y. J. Kim, S. K. Kwak, J.-W. Yoo, J.-B. Baek, *Angew. Chem. Int. Ed.* **2021**, *60*, 17191- 17197.

[22] Y. Su, Y. Wan, H. Xu, K.-i. Otake, X. Tang, L. Huang, S. Kitagawa, C. Gu, *J. Am. Chem. Soc.* **2020**, *142*, 13316-13321.

[23] H. S. Sasmal, A. K. Mahato, P. Majumder, R. Banerjee, *J. Am. Chem. Soc.* **2022**, *144*, 11482.

[24] Y. Li, H. Wang, L. Wang, F. Zhou, Y. Chen, B. Li, Y. Yang, *Nanotechnology* **2011**, *22*, 135605.

[25] K. Koner, S. Karak, S. Kandambeth, S. Karak, N. Thomas, L. Leanza, C. Perego, L. Pesce, R. Capelli, M. Moun, M. Bhakar, T. Ajithkumar, G. Pavan, R. Banerjee, *Nat. Chem.* **2022**, *14*, 507-514.

[26] B. Martial, T. Lefèvre, T. Buffeteau, M. Auger, *ACS Nano* **2019**, *13*, 3232-3242.

[27] S. Cai, B. Sun, X. Li, Y. Yan, A. Navarro, A. Garzon-Ruiz, H. Mao, R. Chatterjee, J. Yano, C. Zhu, J. A. Reimer, S. Zheng, J. Fan, W. Zhang, Y. Liu, *ACS Appl. Mater. Interfaces* **2020**, *12*, 19054-19061.

[28] a) H. Chen, Z.-G. Gu, J. Zhang, *J. Am. Chem. Soc.* **2022**, *144*, 7245-7252; b) C. Du, X. F. Zhu, C. C. Yang, M. H. Liu, *Angew. Chem., Int. Ed.* **2022**, *61*, e202113979.

Entry for the Table of Contents

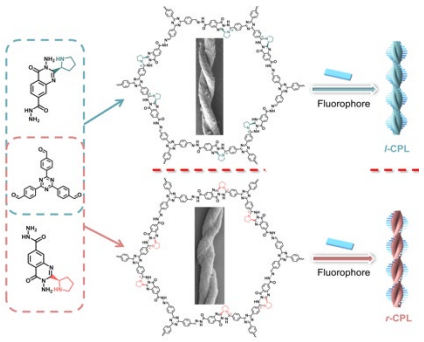

Two chiral COFs with well-defined, one-handed double-helical nanofibrous morphologies are constructed for the first time involving a chiral aminal linkage. By adjusting the amount of acetic acid during synthesis, the helicity of the resulting COF double helices can be readily inversed. Circularly polarized luminescence of the COF double helices is achieved via transferring chirality to achiral fluorophores.